Enhanced permeation of single-file water molecules across a noncylindrical nanochannel

X. W. Meng (孟现文) and J. P. Huang (黄吉平)*
Department of Physics and State Key Laboratory of Surface Physics, Fudan University, Shanghai 200433, China
(Received 13 March 2013; published 29 July 2013)

We utilize molecular dynamics simulations to study the effect of noncylindrical shapes of a nanochannel (which are inspired from the shape of real biological water nanochannels) on the permeation of single-file water molecules across the nanochannel. Compared with the cylindrical shape that has been tremendously adopted in the literature, the noncylindrical shapes play a crucial role in enhancing water permeation. Remarkably, the maximal enhancement ratio reaches a value of 6.28 (enhancement behavior). Meanwhile, the enhancement becomes saturated when the volume of the noncylindrical shape continues to increase (saturation behavior). The analysis of average diffusivity of water molecules helps to reveal the mechanism underlying the two behaviors whereas Poiseuille's law fails to explain them. These results pave a way for designing high-flow nanochannels and provide insight into water permeation across biological water nanochannels.

DOI: 10.1103/PhysRevE.88.014104 PACS number(s): 05.40.−a, 47.61.−k, 05.60.−k, 61.20.Ja

I. INTRODUCTION

The study on the flow of water across nanochannels or microchannels has many applications, e.g., for understanding biological activities [1–8], for designing nanodevices or nanomachines [6,9–11], and even for studying the coalescence of Pickering emulsion droplets [12]. For example, it was found that the measured water flow across nanotubes exceeded values calculated from continuum hydrodynamics models by more than three orders of magnitude and that water permeation abilities of these nanotube-based membranes were several orders of magnitude higher than those of commercial polycarbonate membranes [13]. As a result, a lot of energy will be saved if nanotubes can be used in seawater desalination [14] or water purification [15,16]. Meanwhile, such nanochannels have also been used as model systems to explore some basic behaviors of biological water nanochannels [6,17–21]. The behaviors of water molecules in a carbon nanotube share some phenomena with those inside biological water nanochannels, such as the single-file arrangement [22,23], wavelike density distribution [24,25], wet-dry transition [21], and gating [17,18].

In practice, the noncylindrical shape of nanochannels is usually indispensable. Such nanochannels play important roles in selecting permeation of water or ions [26,27]. For instance, the *Escherichia coli* glycerol uptake facilitator is a noncylindrical channel protein, which transports water, but excludes charged solutes [26]. Also, the voltage-sensitive sodium channel has a bell-shaped structure [28]. However, how the noncylindrical shape of nanochannels affects water permeation has rarely been discussed. It is widely accepted that the external conditions of the nanochannel system greatly affect the permeation of water molecules. So, many external conditions (say, adding external mechanical forces, pressure gradient, or electric fields or charges) have received much attention in the field for studying the transportation of water molecules through nanochannels, while taking the nanochannel shape to be cylindrical [29–40]. Recently, a new particle separation mechanism has been reported according to the combined action of a driving force and an entropic rectification of the Brownian fluctuations caused by the asymmetric shape of the channel [41]. This further encourages us to investigate the effect of nanochannel shapes on water transportation. Without loss of generality, following the approximated cone-shaped water channel between two Pickering emulsion droplets experimentally studied in our recent work [12], here we design a cone-shaped nanochannel as a model noncylindrical nanochannel (see Fig. 1).

II. METHODOLOGY

For our purpose, we resort to molecular dynamics simulations, which have been widely used for studying water dynamics in single-walled carbon nanotubes (SWCNTs), in proteins, and in-between proteins [42–46]. Our simulation framework is shown in Fig. 1(a): two parallel graphite sheets with separation 3.480 nm divide the full space into three parts. There exists a cone-shaped SWCNT between the two graphite sheets, whose construction details are given in Fig. 1(b). The cone-shaped SWCNT is made of two Z-directed, uncapped, (10,0) SWCNTs, each with diameter 0.772 nm and length 1.0 nm, and one nanocone area with length 1.48 nm. Note the nanocone area actually corresponds to two nanocones, each with a length of 0.74 nm [see Fig. 1(b)]. Also, it is worth mentioning that each end of the cone-shaped SWCNT only allows a single water molecule to enter or exit, thus yielding the transportation of single-file water molecules of our interest. The Lennard-Jones (LJ) potential parameters of carbon atoms come from Ref. [21]. The cone-shaped SWCNT and graphite sheets are solvated in a water box (4.652 nm × 4.646 nm × 5.580 nm) with 1148 water molecules; between the two graphite sheets, there are no water molecules outside the cone-shaped SWCNT. The TiP3P water molecule model is used for simulations [42]. In order to prevent the SWCNT and graphite sheets from being swept away, all the carbon atoms are frozen at their original lattices in the simulations. We perform molecular dynamics simulations with GROMACS 3.3.1, and adopt the thermostat of Nosé and Hoover [47,48] with a time constant of 0.5 ps. All simulations are carried out under the NVT ensemble (constant number of molecules, constant volume,

*jphuang@fudan.edu.cn

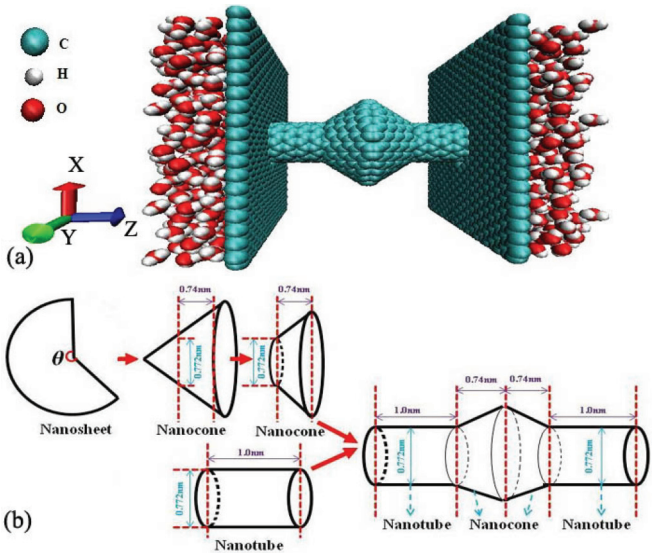

FIG. 1. (Color online) (a) A snapshot of the simulation system with one Z-directed nanochannel (namely, a nanotube-nanocone-nanotube with the cylindrical-cone-cylindrical shape, which we call "cone-shaped SWCNT" for simplicity) perpendicularly joining the centers of two graphite sheets. Atoms are shown in different colors (or gray scale); (b) the details for constructing the cone-shaped SWCNT. Note the Z-directed length of the nanocone area between the two nanotubes is fixed for all θ's throughout this work. Clearly, a larger angle of a graphite nanosheet, θ, corresponds to a larger volume (interior space) of the nanocone area. Incidently, $\theta = 0^\circ$ stands for the case where the whole SWCNT between the two graphite sheets has a cylindrical shape.

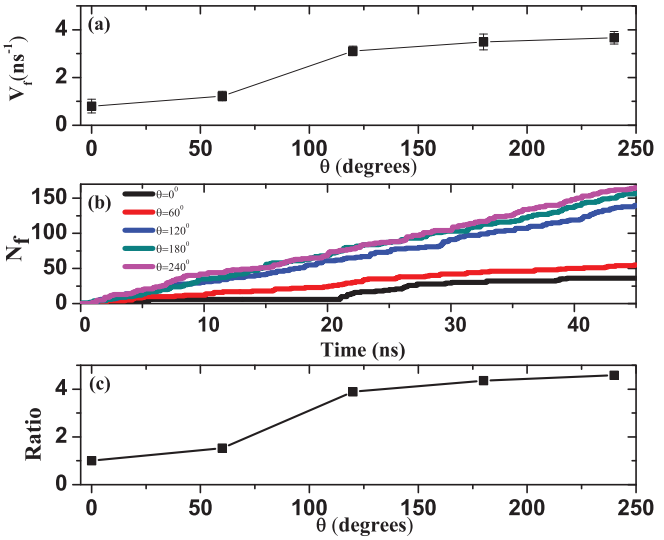

FIG. 2. (Color online) (a) The average rate of transfer of water molecules, V_f, flowing across the cone-shaped SWCNT as a function of θ. Error bars are included. (b) The number of water molecules, N_f, flowing across the cone-shaped SWCNT as a function of time when θ varies from 0° to 240°. (c) Enhancement ratio versus θ. Here, the enhancement ratio is just the ratio between N_f of each θ and that of $\theta = 0^\circ$ at time 45 ns as displayed in (b). The curves in (a) and (c) are a guide to the eye.

and constant temperature). Periodic boundary conditions are applied to all three directions of the simulations box. The initial atomic velocities are generated by a Maxwellian distribution at the temperature of 300 K. The time step is set to be 2 fs, and the total simulation time is 50 ns (the first 5 ns is used for equilibration and the remaining 45 ns are used for statistics). The particle-mesh Ewald [49] method is used for the long-range electrostatic interaction and the cut-off distance for LJ forces is set to be 1.4 nm.

III. RESULTS

Figure 2(a) shows the average rate of transfer of water molecules, V_f, flowing across the cone-shaped SWCNT as a function of θ. The V_f is computed by $V_f = N(t)/t$, where $t = 5$ ns and $N(t) = (1/9)\sum_{k=1}^{9} N_k(t)$. Here, $N_k(t)$ is the number of water molecules transported across the cone-shaped SWCNT either from right to left or from left to right within the statistic time $t = 5$ ns. Clearly, for the total statistical simulation time of 45 ns, $N_k(t)$ have nine values. Figure 2(a) shows V_f increases as θ increases. It is worth noting that increasing θ corresponds to an increasing volume of the nanocone area in the cone-shaped SWCNT. Thus, the water permeation ability of the cone-shaped SWCNT increases as the volume of the nanocone area increases. In detail, as shown in Fig. 2(a), the average rate of transfer of water molecules across the cone-shaped SWCNT is 0.8 ns^{-1} when $\theta = 0^\circ$. As θ increases, the volume of the nanocone area increases, and the permeation ability of water molecules is enhanced greatly. When $\theta = 240^\circ$, the average rate of transfer of water molecules across the SWCNT increases up to 3.667 ns^{-1}. That is, the enhancement ratio reaches a value of 4.58. To display the dynamic behavior behind Fig. 2(a), we plot Fig. 2(b), which shows the number of water molecules transported across the SWCNT, N_f, as a function of time (from 0 to 45 ns) when θ ranges from 0° to 240°. We notice that N_f is different for the five cases, each having a certain θ. Particularly, for $\theta = 0^\circ$, water molecules are transported across the SWCNT fitfully. That is, there is a period of time when no water molecules are transported across the SWCNT. However, as θ increases, the water permeation ability is greatly enhanced. For example, when $\theta = 240^\circ$, water molecules are transported across the SWCNT much more continuously. In other words, water molecules can be more easily transported across the SWCNT when θ increases. Additionally, in order to quantitatively display the enhancement behavior of Figs. 2(a) and 2(b), we plot Fig. 2(c), which shows the enhancement ratio as a function of θ. Evidently, the enhancement ratio increases as θ increases; we call this "enhancement behavior." It should be noted that the enhancement ratio tends to be saturated as θ is large enough; we call this "saturation behavior."

To understand the results shown in Fig. 2, we first display the density probability distributions of water molecules in the cone-shaped SWCNT (see Fig. 3). Because increasing θ corresponds to an increasing volume (interior space) of the nanocone area in the cone-shaped SWCNT, more water molecules can be attracted into the nanocone area for the case of larger θ. As a result, different density probability distributions of water molecules begin to appear for different θ's. For $\theta = 0^\circ$, the probability distribution of water molecules is almost uniform (with only small fluctuations) within the

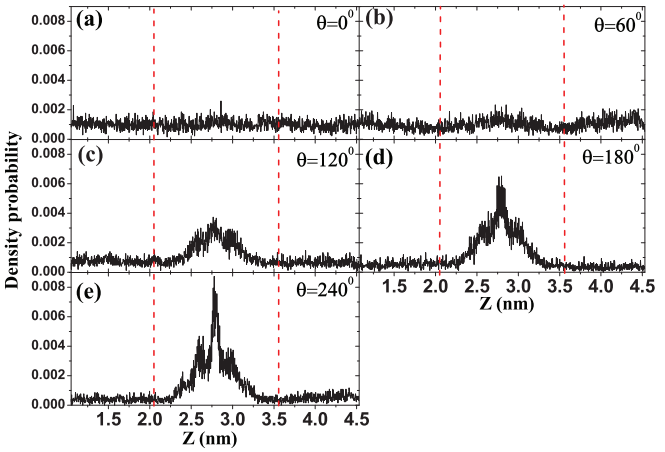

FIG. 3. (Color online) The density probability distributions of water molecules inside the cone-shaped SWCNT versus positions, Z, when θ changes from 0° to 240°. The area between the two vertical dashed lines denotes the position of the nanocone area in the SWCNT with $\theta > 0°$.

whole range of the SWCNT. However, an evident distribution peak in the nanocone area comes to appear as $\theta \geqslant 120°$. Moreover, a larger θ yields a higher peak. The results shown in Fig. 3 agree with our intuition. But, why can more water molecules in the nanocone area enhance the water permeation ability of the SWCNT? Also, why can the enhancement ratio be saturated?

To answer the above questions, we need to analyze the average diffusivity, D, of water molecules within the cone-shaped SWCNT. Details are as follows.

We calculate D according to both the Einstein expression for diffusivity and the Green-Kubo formula [50],

$$D = \frac{1}{450}\sum_{i=1}^{450}\left(\frac{1}{6N_i(t_i - t_{i-1})}\sum_{j=1}^{N_i}|r_j(t_i) - r_j(t_{i-1})|^2\right),$$

where $t_i - t_{i-1} = 0.1$ ns denotes the time step within the whole statistical time 45 ns, thus yielding $t_1 = 0.1$ ns and $t_{450} = 45$ ns. Here, $r_j(t_i)$ is the position of the jth water molecule at t_i, and N_i is the number of water molecules within the cone-shaped SWCNT at t_i. The three components of D along the X, Y, and Z axes are denoted by D_X, D_Y, and D_Z, respectively [see Fig. 4(a)]. Both D_X and D_Y increase with increasing θ. However, D_Z increases when $\theta \leqslant 120°$, but decreases when $\theta > 120°$. From Fig. 4(b), we observe that the average number, N, of water molecules within the cone-shaped SWCNT increases with increasing θ. Because both D_Z and N increase when $\theta \leqslant 120°$, the number of water molecules across the cone-shaped SWCNT must increase, thus yielding an enhanced permeation as shown in Fig. 2. This explains the enhancement behavior. On the other hand, when $\theta > 120°$, N still increases in the cone-shaped SWCNT [see Fig. 4(b)]. However, in this case, D_Z decreases with increasing θ [see Fig. 4(a)]. As a result, the flow rate of water molecules tends to a saturated state [see Fig. 2(a)]. This explains the saturation behavior. In other words, a much larger volume of the nanocone area may not yield a stronger enhancement of permeation of water molecules across the

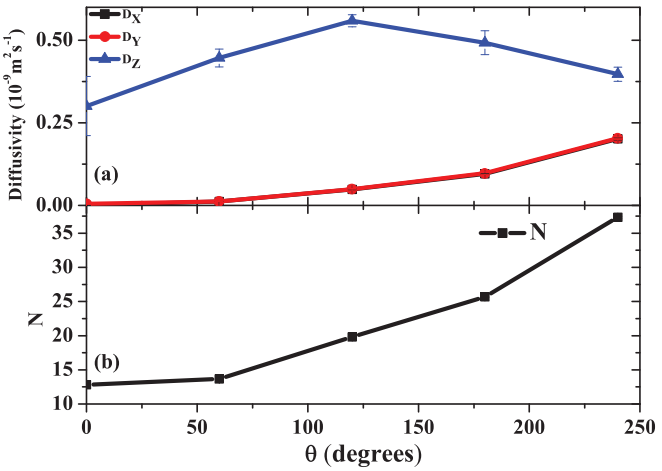

FIG. 4. (Color online) (a) shows the three components D_X, D_Y, and D_Z of the average diffusivity of water molecules within the nanochannel as a function of θ, along the X, Y, and Z axes, respectively. The two curves for D_X and D_Y are overlapped because the nanochannel is symmetrical with respect to the X and Y axes. (b) shows the average number, N, of water molecules within the cone-shaped SWCNT as a function of θ. The solid lines in both (a) and (b) are a guide to the eye. Error bars are included in both (a) and (b); the error bar is smaller than the symbol point for both D_X and D_Y in (a) and for N in (b).

cone-shaped SWCNT. It is worth mentioning that one may insist on using Poiseuille's law to intuitively account for both the enhancement behavior and the saturation behavior. But, the law holds for continuum hydrodynamics, and it is generally inappropriate for the present case at the atomic level [13]. In this case, even though according to the law, the basic idea that a narrower nanochannel will transmit water more slowly than a wider nanochannel seems incontrovertible, it can only partly explain the enhancement behavior instead of the saturation behavior.

Owing to the above analysis based on Figs. 3 and 4, one may infer that more nanocone areas in a cone-shaped SWCNT might help to enhance the water flow up to a higher value.

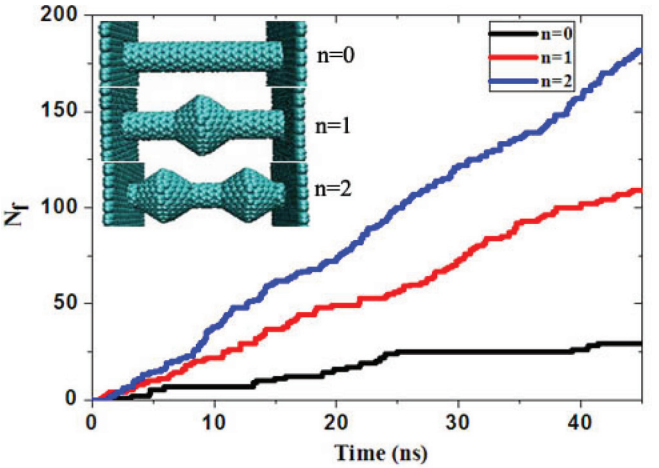

FIG. 5. (Color online) The number of water molecules, N_f, flowing across the cone-shaped SWCNT as a function of time, for different numbers of nanocone areas, n.

Nevertheless, is this true? To answer this question, we attempt to extend the SWCNT length to 4.580 nm, which is long enough to include as many as two nanocone areas (namely, $n = 2$, where n denotes the number of nanocone areas in a cone-shaped SWCNT). Figure 5 shows our simulated results for $\theta = 240^\circ$. As shown in this figure, 29 water molecules are transported across the SWCNT for $n = 0$ (within 45 ns). Interestingly, 109 water molecules and 182 water molecules are transported for $n = 1$ and $n = 2$, respectively. Clearly, the enhancement ratio reaches a remarkable value of 6.28. That is, the permeation ability of water molecules across the cone-shaped SWCNT is enhanced as n increases. An analysis similar to the above applies.

IV. DISCUSSION AND CONCLUSION

In summary, compared with the cylindrical shape of nanochannels (that has been extensively used in the literature), the noncylindrical shape (as inspired from the shape of real biological water nanochannels) has an evident effect on the enhancement of water permeation. Remarkably, the enhancement ratio for the cone-shaped SWCNT with two nanocone areas reaches a value of 6.28 (Fig. 5). Also, the enhancement ratio tends to be saturated as the volume of the nanocone area is large enough (say, $\theta = 180^\circ$ and 240° in Fig. 2). We attribute these results to the coupling between the average diffusivity and the average number of water molecules within the cone-shaped SWCNT along the Z axis whereas Poiseuille's law fails to explain them. It should be noted that if the nanochannels are semiconductors [51], the screening effect does not affect our results because the electrostatic interactions of the water molecules inside the nanochannel remain unchanged. For the same reason, the water permeation properties across a single-walled nanochannel should be the same as those across a multiwalled nanochannel. Our findings may be helpful for designing high-flow nanochannels in water purification and for providing insights into the role of biological nanochannel shapes in water permeation.

ACKNOWLEDGMENTS

We acknowledge the financial support provided by the National Natural Science Foundation of China under Grants No. 11075035 and No. 11222544, by the Fok Ying Tung Education Foundation under Grant No. 131008, by the Program for New Century Excellent Talents in University, by the Shanghai Rising-Star Program (No. 12QA1400200), and by the CNKBRSF under Grant No. 2011CB922004. The computational resources utilized in this research were provided by Shanghai Supercomputer Center.

[1] B. L. de Groot and H. Grubmüller, Science **294**, 2353 (2001).
[2] B. M. Denker, B. L. Smith, F. P. Kuhajda, and P. Agre, J. Biol. Chem. **263**, 15634 (1988).
[3] G. M. Preston and P. Agre, Proc. Natl. Acad. Sci. USA **88**, 11110 (1991).
[4] M. L. Zeidel, S. V. Ambudkar, B. L. Smith, and P. Agre, Biochemistry **31**, 7436 (1992).
[5] K. Wood, M. Plazanet, F. Gable, B. Kessler, D. Oesterhelt, D. J. Tobias, G. Zaccai, and M. Weik, Proc. Natl. Acad. Sci. USA **104**, 18049 (2007).
[6] X. Gong, J. Li, H. Zhang, R. Wan, H. Lu, S. Wang, and H. Fang, Phys. Rev. Lett. **101**, 257801 (2008).
[7] B. X. Xu, Y. B. Li, T. Park, and X. Chen, J. Chem. Phys. **135**, 144703 (2011).
[8] X. Y. Li, Y. C. Shi, Y. L. Yang, H. L. Du, R. H. Zhou, and Y. L. Zhao, J. Chem. Phys. **136**, 175101 (2012).
[9] K. Besteman, J. O. Lee, F. J. Wiertz, H. A. Heering, and C. Dekker, Nano Lett. **3**, 727 (2003).
[10] M. F. L. De Volder, S. H. Tawfick, R. H. Baughman, and A. J. Hart, Science **339**, 535 (2013).
[11] I. Hanasaki, T. Yonebayashi, and S. Kawano, Phys. Rev. E **79**, 046307 (2009).
[12] G. Chen, P. Tan, S. Chen, J. P. Huang, W. Wen, and L. Xu, Phys. Rev. Lett. **110**, 064502 (2013).
[13] J. K. Holt, H. G. Park, Y. M. Wang, M. Stadermann, A. B. Artyukhin, C. P. Grigoropoulos, A. Noy, and A. Bakajin, Science **312**, 1034 (2006).
[14] R. F. Service, Science **313**, 1088 (2006).
[15] A. T. Nasrabadi and M. Foroutan, Desalination **277**, 236 (2011).
[16] X. B. Wang, L. Jin, W. Z. Xu, T. Cao, X. J. Song, and S. L. Cheng, Micro Nano Lett. **7**, 918 (2012).
[17] J. Y. Li, X. J. Gong, H. J. Lu, D. Li, and R. H. Zhou, Proc. Natl. Acad. Sci. USA **104**, 3687 (2007).
[18] X. W. Meng, Y. Wang, Y. J. Zhao, and J. P. Huang, J. Phys. Chem. B **115**, 4768 (2011).
[19] X. J. Gong, J. Y. Li, H. J. Lu, R. Z. Wan, J. C. Li, J. Hu, and H. P. Fang, Nat. Nanotechnol. **2**, 709 (2007).
[20] R. Z. Wan, J. Y. Li, H. J. Lu, and H. P. Fang, J. Am. Chem. Soc. **127**, 7166 (2005).
[21] G. Hummer, J. C. Rasaiah, and J. P. Noworyta, Nature (London) **414**, 188 (2001).
[22] S. Cambre, B. Schoeters, S. Luyckx, E. Goovaerts, and W. Wenseleers, Phys. Rev. Lett. **104**, 207401 (2010).
[23] Y. Wang, Y. J. Zhao, and J. P. Huang, J. Phys. Chem. B **115**, 13275 (2001).
[24] J. Y. Su and H. X. Guo, ACS Nano **5**, 351 (2011).
[25] H. Lu, J. Li, X. Gong, R. Wan, L. Zeng, and H. Fang, Phys. Rev. B **77**, 174115 (2008).
[26] I. Kosztin and K. Schulten, Phys. Rev. Lett. **93**, 238102 (2004).
[27] Z. Siwy, I. D. Kosinska, A. Fulinski, and C. R. Martin, Phys. Rev. Lett. **94**, 048102 (2005).
[28] C. Sato, Y. Ueno, K. Asai, K. Takahashi, M. Sato, A. Engel, and Y. Fujiyoshi, Nature (London) **409**, 1047 (2001).
[29] M. K. Chaudhury and G. M. Whitesides, Science **256**, 1539 (1992).
[30] H. Linke, B. J. Alemán, L. D. Melling, M. J. Taormina, M. J. Francis, C. C. Dow-Hygelund, V. Narayanan, R. P. Taylor, and A. Stout, Phys. Rev. Lett. **96**, 154502 (2006).

[31] J. R. Bordin, A. Diehl, M. C. Barbosa, and Y. Levin, Phys. Rev. E **85**, 031914 (2012).
[32] J. B. Zhao, L. Liu, P. J. Culligan, and X. Chen, Phys. Rev. E **80**, 061206 (2009).
[33] M. D. Ma, L. M. Shen, J. Sheridan, J. Z. Liu, C. Chen, and Q. S. Zheng, Phys. Rev. E **83**, 036316 (2011).
[34] K. Falk, F. Sedlmeier, L. Joly, R. R. Netz, and L. Bocquet, Nano Lett. **10**, 4067 (2010).
[35] A. Kalra, S. Garde, and G. Hummer, Proc. Natl. Acad. Sci. USA **100**, 10175 (2003).
[36] T. A. Pascal, W. A. Goddard, and Y. S. Jung, Proc. Natl. Acad. Sci. USA **108**, 11794 (2011).
[37] J. H. Walther, T. Werder, R. L. Jaffe, and P. Koumoutsakos, Phys. Rev. E **69**, 062201 (2004).
[38] B. K. Agrawal, V. Singh, A. Pathak, and R. Srivastava, Phys. Rev. B **75**, 195421 (2007).
[39] J. S. Babu and S. P. Sathian, Phys. Rev. E **85**, 051205 (2012).
[40] Y. C. Liu and Q. Wang, Phys. Rev. B **72**, 085420 (2005).
[41] D. Reguera, A. Luque, P. S. Burada, G. Schmid, J. M. Rubí, and P. Hänggi, Phys. Rev. Lett. **108**, 020604 (2012).
[42] W. L. Jorgensen, J. Chandrasekhar, J. D. Madura, R. W. Impey, and M. L. Klein, J. Chem. Phys. **79**, 926 (1983).
[43] D. J. Mann and M. D. Halls, Phys. Rev. Lett. **90**, 195503 (2003).
[44] B. Y. Wang and P. Kral, Phys. Rev. Lett. **101**, 046103 (2008).
[45] C. Chen, M. Ma, K. Jin, J. Z. Liu, L. Shen, Q. Zheng, and Z. Xu, Phys. Rev. E **84**, 046314 (2011).
[46] P. Tangney, S. G. Louie, and M. L. Cohen, Phys. Rev. Lett. **93**, 065503 (2004).
[47] S. Nosé, J. Chem. Phys. **81**, 511 (1984).
[48] W. G. Hoover, Phys. Rev. A **31**, 1695 (1985).
[49] T. A. Darden, D. M. York, and L. G. Pedersen, J. Chem. Phys. **98**, 10089 (1993).
[50] C. Rapaport, *The Art of Molecular Dynamics Simulation* (Cambridge University Press, Cambridge, UK, 1995).
[51] B. Kozinsky and N. Marzari, Phys. Rev. Lett. **96**, 166801 (2006).